Pinholes in antiferromagnetically coupled multilayers: Effects on hysteresis loops and relation to biquadratic exchange

J. F. Bobo
LPMC, UMR 5830 CNRS-UPS-INSA, INSA, Département de Génie Physique, 31077 Toulouse Cedex 4, France

H. Kikuchi
Fujitsu Limited, 10-1 Morinosato-Wakamiya, Atsugi, 243-01, Japan

O. Redon
Laboratoire Louis Néel, CNRS, 25, Avenue des Martyrs, Boîte Postale 166, 38042 Grenoble Cedex 9, France

E. Snoeck
CEMES-CNRS, 29, rue Jeanne Marvig, 31055 Toulouse Cedex, France

M. Piecuch
LPM, UMR CNRS 7556, Université Henri Poincaré, Boîte Postale 239, 54506 Vandœuvre Cedex, France

R. L. White
Department of Materials Science and Engineering–CRISM, Stanford University, Stanford, California 94305-2205
(Received 29 April 1998; revised manuscript received 3 November 1998)

We present a micromagnetic study of the influence of ferromagnetic bridges between consecutive ferromagnetic layers in antiferromagnetically coupled multilayers. The model is compared with experimental results for hysteresis loops obtained from the multilayer systems Co-Cu and FeNi-Ag. The presence of pinholes in Cu-Co multilayers is confirmed by transmission electron microscopy. We demonstrate that low densities of ferromagnetic pinholes in such multilayers are sufficient to give rise to significant deviations from the expected bilinear interlayer coupling and modify the observed interlayer oscillatory exchange coupling. The effects of pinholes can be simulated in certain cases by biquadratic exchange coupling, and we propose a magnetic phase diagram which correlates the apparent bilinear and biquadratic couplings to the pinholes density, size, and interlayer exchange strength. [S0163-1829(99)14529-6]

I. INTRODUCTION

The presence of holes in a nanometer-scale thin film is commonly believed to occur. The origin of pinholes may be due to fundamental growth processes [e.g., Stransky-Krastanov or island growth in multilayers, inducing roughness and holes, or twinning faults in molecular beam epitaxy (MBE) grown samples] or to more extrinsic origins like the presence of arrays of dislocations or the morphology of the substrate (pits, steps, terraces). For a single-layer film such holes may not play a significant role in determining the film properties. However, if a multilayer structure is grown with such defects, one can easily imagine that the holes in one of the layers will get filled by the material of the subsequent layer, producing an electrical or magnetic interlayer coupling affecting significantly the properties of the whole structure. We will calculate the effect of such pinhole defects in antiferromagnetically (AF) coupled multilayers, and we will compare it to the experimental magnetic behavior of real samples.

II. DESCRIPTION OF THE PROBLEM

Interlayer magnetic exchange coupling in multilayers (or trilayers) comprised of a succession of ferromagnetic and nonmagnetic layers has been observed in a wide range of systems based on transition metals.[1] Such interlayer coupling is at the origin of the so-called giant magnetoresistance[2,3] (GMR) in multilayers. A study of the dependence of this exchange coupling upon the thickness of the nonmagnetic (or spacer) layers shows an oscillatory behavior with a first maximum of antiferromagnetic coupling occurring at spacer thicknesses (t_s) between 6 and 15 Å for most spacer materials. Usually, the maximum GMR is observed near this first maximum. Camley and Barnas[4] have shown theoretically and Diény *et al.*[5] experimentally that the GMR effect is proportional to $\cos 2\theta$, where 2θ is the angle between the magnetizations of successive ferromagnetic layers in zero field (this angle becomes 0 at the saturation field). Thus the zero-field value of 2θ has to be as close as possible to 180° to achieve the maximum GMR. The experimentally observed magnetization curves of AF-coupled multilayers can show several behaviors, as summarized in Fig. 1 for two Cu-Co multilayers with equal Co thickness (12 Å) and a Cu spacer layer thickness equal to 7 and 9 Å. In the ideal case of bilinear uniform antiferromagnetic exchange, the magnetization curve is a straight line with no remanence illustrated in Fig. 1(a). The saturation field H_S is then simply proportional to the interlayer coupling intensity J_i. However, this linear behavior is rarely observed at the first AF maximum [see

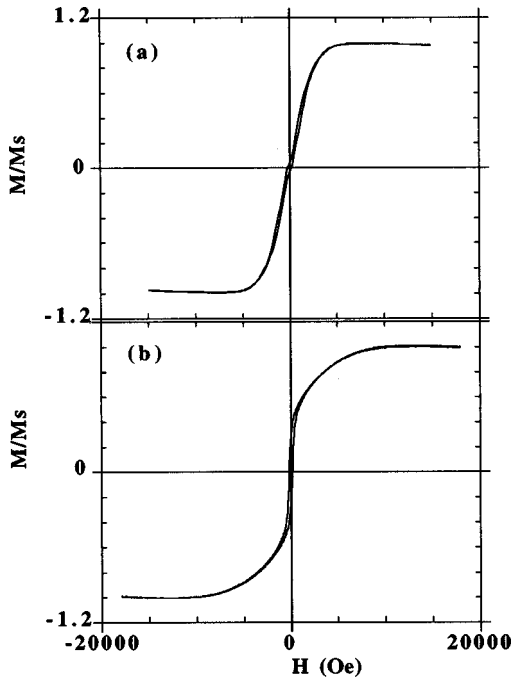

FIG. 1. Magnetization curves obtained at room temperature for two Co(12 Å)-Cu(t_s) multilayers with, respectively, $t_s = 9$ Å (a) and $t_s = 7$ Å (b).

Fig. 1(b)] and, as developed further, corrective coupling terms are introduced to fit the experimental data. The usual expression for the free energy of a multilayer with an interlayer coupling J_{ij} between consecutive ferromagnetic layers indexed by i and j having equal thickness t_m and bulk saturation magnetization M_S, assuming coherent in-plane rotation of the magnetization within each layer is

$$E = -\frac{1}{2}\sum_{ij} J_{ij}\cos(\theta_i - \theta_j) - M_S t_m H \sum_i \cos\theta_i + E_{\text{anis}}. \quad (1)$$

The parameters of Eq. (1) are displayed in Fig. 2. Note that the angles θ are referenced with respect to the applied magnetic field. The first term of Eq. (1) is the usual bilinear exchange, the second term is the Zeeman term, and E_{anis} is the anisotropy contribution. The magnetic anisotropy can be either intrinsic magnetocrystalline or can be induced by the

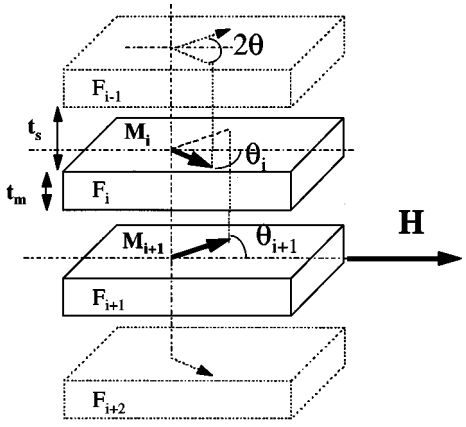

FIG. 2. Schematic view of a multilayer with interlayer exchange coupling.

processing conditions of the multilayer. We will neglect the anisotropy energy in this study, assuming that the Zeeman and exchange contributions dominate. If we assume all layers are identical, the coupling occurs mainly between neighbor layers, and $\theta_{i-1} = \theta_{i+1} = -\theta_i = -\theta$. Equation (1) is simplified as

$$E = -(N-1)J\cos 2\theta - NM_S t_m H\cos\theta. \quad (2)$$

The minimization of Eq. (2) then gives linear magnetization curves displayed in Fig. 1(a) with a saturation field:

$$H_{\text{sat}} = \frac{4(N-1)|J|}{NM_S t_m}. \quad (3)$$

However, this simplified description of interlayer exchange coupling does not describe correctly the shape of experimentally observed magnetization or GMR curves. For most cases the hysteresis loops have a non-negligible remanence and curvature [Fig. 1(b)]. Such hysteresis loops can frequently be fitted by a model that includes a biquadratic interlayer exchange. This biquadratic term has been initially proposed by Rührig *et al.* in the case of exchange-coupled multilayers[6] and has been reported by other authors:[7]

$$E = -Nt_m M_S H\cos\theta - (N-1)(J\cos 2\theta + B\cos^2 2\theta). \quad (4)$$

The term B ($B<0$) takes into account the biquadratic coupling. Biquadratic coupling leads basically to perpendicular zero-field configurations of the spins ($\varphi_i = \theta_i - \theta_{i+1} = 2\theta = 90°$) compared to the bilinear coupling which causes antiparallel configurations ($\varphi_i = \theta_i - \theta_{i+1} = 2\theta = 180°$). Several origins have been proposed for the biquadratic term, either as an intrinsic effect related to the interlayer coupling mechanism[8] or due to extrinsic effects related to the morphology of the multilayer. In the latter case and for Fe-Cr multilayers, Slonczewski demonstrated that the presence of atomic steps in the Cr spacer layer could cause an apparent biquadratic coupling.[9] His model is based on the bulk antiferromagnetism of Cr which causes small periodicity coupling oscillations versus the chromium spacer layer thickness [period of ≈2 monolayers (ML) ≈4 Å]. If there is an atomic step in the spacer layer, then the sign of the interlayer coupling will change from positive [ferromagnetic (F)] to negative (AF). A periodic array of steps will therefore induce fluctuations of the interlayer coupling. If the size of the terraces is smaller than some critical length, Slonczewski's model predicts a behavior of the magnetization curves which can be fitted by the introduction of a biquadratic interlayer exchange coupling. Several authors[10,11] have reported the fitting of hysteresis curves to energy expressions involving biquadratic terms. They report cases for which the biquadratic exchange coefficient is comparable to or even larger than the bilinear term. No theory based on fundamental interactions presently predicts biquadratic exchange magnitudes approaching those used to fit the magnetization curves in the above. We believe the physical process operative, and producing in many cases a behavior mimicked by biquadratic exchange, is in fact pinhole coupling. The modification of AF coupling by discontinuities in the spacer layers related to their finite size has been invoked by Gradmann and Elmers[12] to explain the controversy between MBE and sputtered Co/Cu(111) samples. We simply assume in our work that spacer

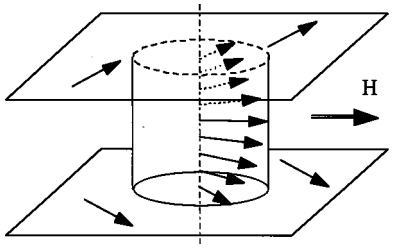

FIG. 3. Schematic view of a pinhole showing the twisting of the magnetization (symbolized by arrows) through the pinhole between the two magnetic layers.

layers of infinite size, but having ferromagnetic discontinuities, can also affect the AF interlayer coupling. This has also been discussed in the early works on magnetic multilayers.[13]

Basically, interlayer coupling through pinholes resembles the theory presented by Slonczewski concerning two films having a primary AF coupling, but with a distribution of F-coupled local regions. However, a major difference is that pinholes couple the ferromagnetic layers by direct exchange, inducing a F coupling far stronger than the AF coupling of the surrounding areas J_{AF} is of the order of several tenths of erg/cm^2,[2,14,15] while J_h is estimated two orders of magnitude higher. If the pinhole is represented by a ferromagnetic column of height t_s (the spacer layer thickness), its magnetization, assumed to remain in plane,[16] will experience a twisting around an axis perpendicular to the two planes (see Fig. 3). The exchange energy cost for such a twisting is then[17]

$$E_{\mathrm{ex}}=\int_V A\left[\left(\frac{\nabla M_x}{M_S}\right)^2+\left(\frac{\nabla M_y}{M_S}\right)^2+\left(\frac{\nabla M_z}{M_S}\right)^2\right]dV$$
$$=S\int_0^{t_s}A\left(\frac{d\varphi}{dz}\right)^2dz=S\int_0^{t_s}A\left(\frac{d2\theta}{dz}\right)^2dz. \tag{5}$$

Performing a micromagnetics integration along the column, one obtains, in a first approximation [$d(2\theta)/dz$ is assumed constant and S is the area occupied by the pinhole],

$$E\approx 4SA\frac{\theta^2}{t_s}\approx\frac{4SA}{t_s}\left(\frac{1-\cos 2\theta}{2}\right)=S\frac{2A}{t_s}-S\frac{2A}{t_s}\cos 2\theta.$$

It gives an effective ferromagnetic interlayer exchange coupling at the pinhole given by Eq. (6):

$$J_h=\frac{2A}{t_s}. \tag{6}$$

Then, if we use commonly accepted constants for the saturation magnetization M_S, the exchange stiffness A ($\approx 10^{-6}$ erg/cm), and a standard value for the spacer layer thickness t_s(≈ 10 Å), one obtains $J_h\approx 20$ erg/cm^2. Therefore, the coupling strength between two ferromagnetic layers through a pinhole is ferromagnetic and between one and two orders of magnitude larger than the AF coupling away from the pinhole. We can develop a model based on a distribution of pinholes in between AF-coupled magnetic multilayers and determine the influence of various parameters such as pinhole size, pinhole density, and the intensity of their coupling to calculate the magnetization curves of magnetic multilayers.

III. PINHOLE MODEL

We use the standard micromagnetics approach to solve the magnetic configuration of a trilayer F_1-spacer-F_2, with F_1 and F_2 the two ferromagnetic layers.[18] This approach can be generalized to a multilayer stack if we assume that all the layers are identical and that the coupling occurs between first neighbor layers only. The energy of the system for N magnetic layers will be the sum of $N-1$ interlayer coupling terms and N Zeeman terms. The interlayer coupling is defined as AF everywhere in the trilayer except on the pinholes sites where it is positive and is given by Eq. (6). Therefore the value of the interlayer exchange coupling will depend on the in-plane location (x,y) across the sample surface. In-plane domain walls will appear between F regions at the pinholes and the surrounding AF areas. The magnetic field is applied in the plane of the layers along the direction x. If we assume, from symmetry, that the magnetizations of the two layers F_1 and F_2 are exactly mirroring each other with respect to the applied magnetic field, we can define $\theta(x,y)$ as the angle between the field axis and the local magnetization direction. Then $\theta_1(x,y)=-\theta_2(x,y)=\theta(x,y)$ and the total energy of a bilayer system can be written as a function of the local angle $\theta(x,y)$:

$$E=\int\int_s[2At_m(\nabla\theta)^2-J(x,y)\cos 2\theta(x,y)$$
$$-2HM_St_m\cos\theta(x,y)]dx\,dy. \tag{7}$$

In the case of a multilayer these energy terms get corrected as presented in Eq. (2). This trilayer approximation, used for a multilayer, does not take into account the possibility that a pinhole could either propagate through the whole multilayer stack or be confined into one fraction of the whole artificial stacking. Transmission electron microscopy [(TEM) (see Sec. V)] indicates that pinholes would not short all the layers through the whole multilayer thickness, and so they have a smaller impact on the total coupling of the multilayer than the AF exchange. Thus we introduced a correction parameter α to the ferromagnetic interlayer coupling at the pinhole sites ($0<\alpha<1$) to reduce the effective pinhole strength. This problem of through-thickness coupling variations has been recently presented by Kolhepp *et al.*[19] in the case of Fe-FeSi multilayers which exhibit a different interlayer coupling at the surface of the multilayer (dominant AF coupling) than at the substrate side (F coupling). They concluded that this inhomogeneous behavior leads to a mimic of biquadratic coupling. The reduction of the pinhole interlayer coupling can also be explained by the small size of the column of the ferromagnet reducing its effective ferromagnetic stiffness. This aspect of the pinhole problem was recently developed by Fulghum and Camley.[20] They used a more sophisticated method to determine the magnetic ground state of a pinhole-coupled structure, calculating the local value and orientation of the spin versus the temperature, the applied field, and the density of pinholes. They demonstrated that the strength of the pinhole coupling is strongly temperature dependent as a direct result of their reduced size. Another reason why we introduce a reduction to the exchange through the pinholes comes from the approximation used to derive J_h in Eq. (6) where we assumed a linear twisting of the spins along the

ferromagnetic column. This assumption is valid for small twisting and perfectly cylindrical columns, but the actual case may lead to lower coupling strength.

IV. SOLUTIONS TO THE PINHOLE MODEL

A. Analytical approach

From Eq. (7), it is possible to write an equivalent Euler's equation:

$$2At_m\nabla^2\theta(x,y)=2J(x,y)\sin\theta(x,y)\cos\theta(x,y) + HM_S t_m \sin\theta(x,y). \quad (8)$$

Equation (8) could not be solved analytically for the as-considered pinhole configuration, but it provides insight of the as expected solution, and so leads to a characteristic length

$$l^2=\frac{At_m}{|J|}, \quad (9)$$

which defines the solution space of the equation. Since there are two distinct domains, l will have two different values: l_h in the pinhole area where J is positive and l_i in the AF area where J is negative. l_i is associated with the domain wall width in the AF area surrounding a pinhole and is the distance of relaxation from the ferromagnetic to the antiferromagnetic alignment from the pinhole to the unpinned region. The concept of the characteristic length l_h or the domain wall width within a pinhole is somewhat more subtle, but can be understood as follows. Imagine a pinhole such that the spins in the magnetic films at the perimeter of the pinhole are fixed in the antiferromagnetic alignment (an unphysical situation, but useful for a gedanken experiment). The ferromagnetic coupling through the pinhole induces a parallel configuration of the spins, therefore rotated by 90° from the orientation in the AF area. If $l_h<r$, the pinhole radius, the spins within the pinhole area will indeed be torqued around so that the spins at or near the center of the pinhole will achieve the ferromagnetic configuration. If $l_h>r$, the spins in the pinhole will be only partially torqued around and will not achieve full ferromagnetic alignment. The parameter $\rho=r/l_h$ is a measure of the rotation of the spins within the pinhole area. A large ρ, achieved when r is large or l_h is small, corresponds to a strong coupling through the pinhole. Inserting this relationship into Eq. (9) and including the pinhole stiffness reduction factor α, we finally obtain

$$l_h^2=\frac{t_m t_s}{2\alpha} \quad \text{with} \quad 0<\alpha<1. \quad (10)$$

Note that the pinhole strength increases for thin spacer layers, as it should. Since J within the pinhole is much larger than J in the antiferromagnetically coupled region, l_h is smaller than l_i. The ratios between, respectively, l_i and the pinhole spacing and between l_h and the pinhole diameter play an important role in characterizing the magnetic behavior of the coupled films. We can estimate the values of l_h and l_i: with standard interlayer exchange coupling values of 0.1–0.8 erg/cm^2, a ferromagnetic exchange stiffness $A \approx 10^{-6}$ erg/cm, and ferromagnetic layers of ≈10–20 Å, $l_i \approx 40-400$ Å, whereas $l_h \approx 5-10$ Å for the usual cases at the maximum AF interlayer exchange occurring commonly for $t_s<10$ Å. The behavior of the system clearly depends on the spacing between pinholes and the strength of the pinhole coupling. As we will subsequently see in Sec. VII, the ratio of d_h, the distance between pinholes, to l_i and the ratio of the pinhole diameter, r $(=a)$, to l_h provide useful parameters for the construction of a phase space in which the solutions to the pinhole model can be classified. Parenthetically, we note that Eq. (8) has been solved analytically for a somewhat simpler quasi-one-dimensional case where the bridging structures are long thin sheets.[21] The magnetization curves and spin configurations for this case are similar to the same properties calculated for the pinhole configuration obtained by the numerical solutions given below.

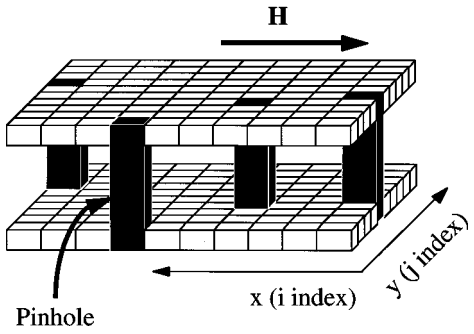

FIG. 4. View of our numerical model. Pinholes (black columns) are randomly scattered over the meshed area. They connect both layers by direct ferromagnetic exchange, while the magnetization in each cell of the mesh is coupled to its first four neighbors by direct exchange and to the other layer cell by indirect antiferromagnetic coupling.

B. Numerical approach

To solve the general case, we created a square meshed area containing up to $n_{\text{cells}}=2500$ cells of lateral size a. A given number of pinholes n_h, each occupying one cell, are each randomly arranged over the meshed area. Periodic boundary conditions are used at the edges of the meshed area (see Fig. 4). The mean distance between two pinholes is $\langle d_h\rangle = a\times\sqrt{n_{\text{cells}}/n_h}$. Size fluctuations of the pinholes were not taken into account by the model, but several runs with constant pinholes densities $x_h=n_h/n_{\text{cell}}$, l_i/l_h ratios and varying l_i/a could be performed to probe the influence of the pinholes sizes. In each cell, indexed by (i,j) the local expression of the energy is given by

$$\frac{E_{ij}}{a^2}=-\frac{NAt_m}{a^2}\sum_{i',j'\ \text{neighbors}}\cos(\theta_{ij}-\theta_{i'j'}) - NM_s t_m H\cos\theta_{ij}-(N-1)J_{ij}\cos 2\theta_{ij}, \quad (11)$$

where the first and last terms are the interlayer and interlayer exchange terms, respectively. J_{ij} is the local value of the interlayer exchange coupling in one cell whose location is specified by the i and j indices (the indices i' and j' represent the neighboring cells in the same layer):

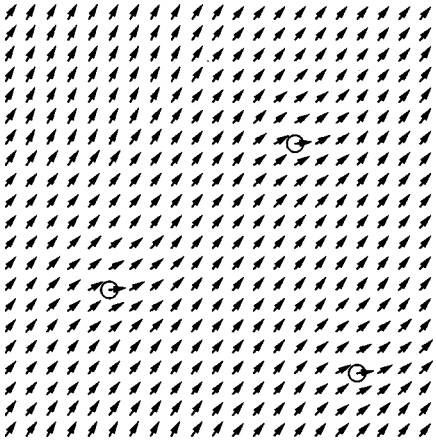

FIG. 5. Zero-field spin configuration of a bilayer with three pinholes (only the top layer is displayed, the field direction is horizontal).

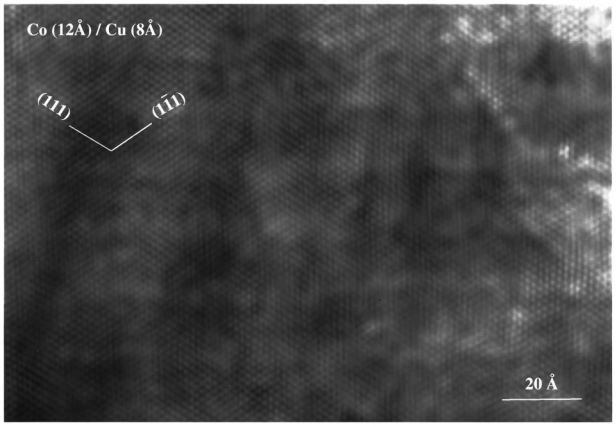

FIG. 6. HRTEM of a Co-Cu multilayer showing the epitaxial growth of Cu and Co, but a very low contrast between the different layers.

(i) $J_{ij}=J_0<0$ outside of pinholes as a result of the AF coupling,

(ii) $J_{ij}=2\times A\times\alpha/t_s>0$ at the pinhole sites.

In order to save computation time, the cosine expressions in Eq. (11) are replaced by the projections along x and y axes of the magnetization unit mean vector ($m_x^{ij}=\cos\theta_{ij}$ and $m_y^{ij}=\sin\theta_{ij}$):

$$\frac{E_{ij}}{a^2}=-\frac{NAt_m}{a^2}\sum_{i',j'}\sum_{\text{neighbors}}(m_x^{ij}m_x^{i'j'}-m_y^{ij}m_y^{i'j'})-NM_st_mHm_x^{ij}-(N-1)J_{ij}(m_x^{ij^2}-m_y^{ij^2}). \quad (12)$$

It is convenient to write this expression in terms of the reduced field $h=H/H_{\text{sat}}$ [where H_{sat} is given by Eq. (3)] and the characteristic lengths l_h and l_i:

$$\frac{E_{ij}}{NAt_m}=-\sum_{i'j'}\sum_{\text{neighbor cells}}(m_x^{ij}m_x^{i'j'}-m_y^{ij}m_y^{i'j'})-4\left(\frac{N-1}{N}\right)\frac{a^2}{l_i^2}hm_x^{ij}-\left(\frac{N-1}{N}\right)\frac{a^2}{l_{ij}^2}(m_x^{ij^2}-m_y^{ij^2}). \quad (13)$$

Note that in the last term of Eq. (13) we have l_{ij}^2 where l_{ij} may have either the value l_i if the cell (i,j) is outside a pinhole or the value l_h if cell (i,j) contains a pinhole.

The total energy was minimized by the torque method[18] which consists of aligning the local magnetization vector along an effective field which is the gradient of the local energy with respect to the magnetization direction: $\vec{m}_{ij}\propto\vec{\mu}_{ij}=-\vec{\nabla}_m(E_{ij})$ recursively at all the sites of the mesh until the discrete magnetization vectors converge to the lowest-energy configuration. Our code[22] makes a minimum of 2000 iterations over the mesh allowing a convergence better than 10^{-6}. For an example of a spin configuration, Fig. 5 shows the remanent magnetic configuration obtained with a Co(12 Å)-Cu(8 Å)-Co(12 Å) trilayer with a pinhole density of 0.0068, a mesh size of 10 Å, and an AF exchange of -0.5 erg/cm^2. The three pinholes presented in this figure are labeled by circles, and only the top layer configuration is reported. The Co underlayer, not shown in this figure, behaves symmetrically with respect to the horizontal magnetic field axis (its spins are therefore pointing downwards). The orientation of the local moment is almost parallel to the applied field in the pinholes while it tends to align perpendicular in the AF area. However, the parameters chosen for this calculation are such that the pseudo-domain-wall in the film (determined by l_i) is greater than the spacing between the pinholes, and so the spins never become perpendicular the H (relaxed entirely to the antiferromagnetic configuration anywhere over the mesh). The equilibrium configuration was obtained this way for each value of the applied magnetic field up to the saturation field (i.e., until all the spins are aligned along the applied field). The total magnetization is defined as the sum over the cells of $M_S\cos\theta$. We used our model to fit the experimental data using J_0, n_h, and α as parameters, and we show[23] that low pinhole area densities are required to fit the experimental magnetization curves.

V. ORIGIN OF PINHOLES: EXPERIMENTAL EVIDENCE BY TRANSMISSION ELECTRON MICROSCOPY

The in-plane morphology of the films was investigated by transmission electron microscopy. The samples presented here were deposited by rf sputtering.[24] We present as most relevant data concerning very thin spacer layer thickness around the first AF maximum of Cu-Co. In order to perform TEM, the samples were first prepared as standard cross-sectional specimens and the final thinning was done by ion milling with a 77-K-cooled sample holder to minimize preparation damage. The micrographs were collected with a Phillips CM 30 microscope operating at 300 kV. As shown in Fig. 6, high-resolution (HR) confirms the epitaxial growth of copper and cobalt. Since cobalt and copper have very close atomic numbers (respectively, $Z=27$ and $Z=29$), they have a low contrast in HRTEM. If TEM is used in out-of-focus conditions to enhance the Fresnel contrast,[25] the stacking of Cu and Co becomes visible as shown in Fig. 7. We can also distinguish discontinuities in the copper layers, which appear darker. These discontinuities occur rather randomly on the cross section and are assumed to be cobalt pinholes. Their size is close to the thickness of the copper layers ($t_s\approx 8$ Å in this sample), and the mean distance be-

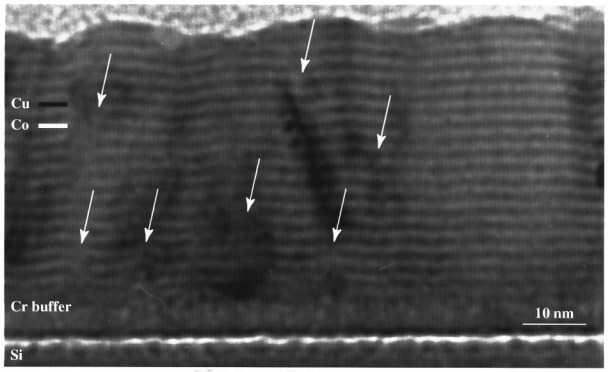

FIG. 7. Defocused TEM micrograph of a Cu-Co multilayer with contrast enhancement between Co and Cu due to Fresnel contrast. Several discontinuities arrowed in the copper layers (pinholes) are visible.

tween two consecutive pinholes is approximately 100 Å. Note that some of these pinholes propagate through several bilayer periods of the stacking. The same kind of behavior is shown in Fig. 8 for another Cu-Co multilayer, confirming the existence of pinholes in Co-Cu multilayers.

VI. MAGNETIZATION CURVES: COMPARISON WITH EXPERIMENT

A. Co/Cu multilayers

These multilayers were deposited by dc magnetron sputtering on oxidized Si(100) wafers.[26] The base pressure and Ar pressure during deposition were 5×10^{-8} Torr and 3.0 mTorr, respectively. The deposition rates were about 1.0 Å/s for Cu and 0.3 Å/2 for Co. The Co(50 Å)/[Cu(t_s Å)/Co(10 Å)]$_N$/Cu(50 Å) films, with t_S in the range from 8.3 to 11.1 Å, were (111) textured. The values of t_S are close to the first peak of the well-known GMR vs Cu thickness curve. The MR ratio was measured using a four-point probe method. The magnetic properties were measured with a vibrating sample magnetometer. Figure 9 shows the $M=f(H)$ curves measured on samples with $N=10$ and the as-calculated ones using the pinhole model. The magnetization

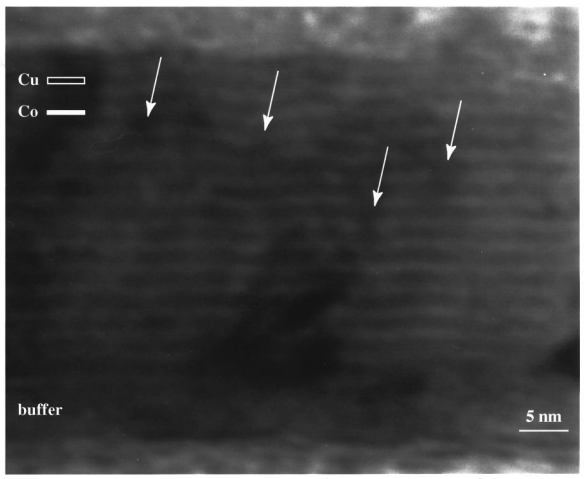

FIG. 8. Fresnel contrast TEM micrograph on another Cu-Co multilayer showing again pinholes.

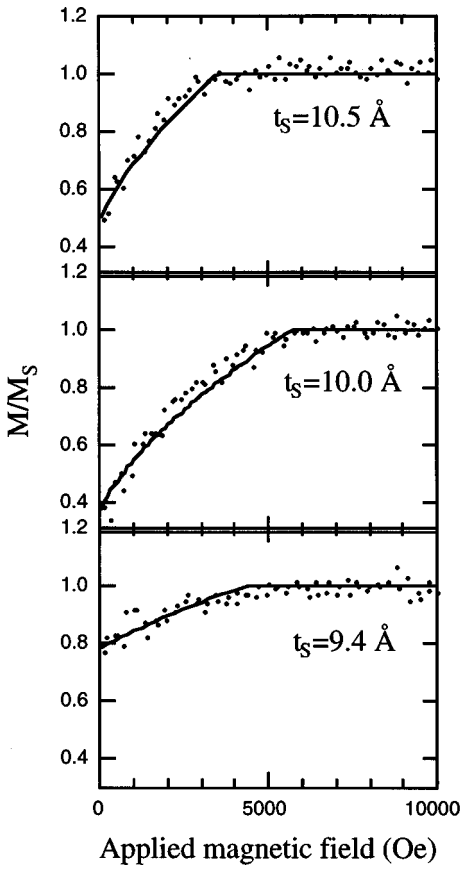

FIG. 9. MH curves for Co-Cu multilayers with ten bilayers at various spacer layer thickness near the first AF peak fitted to the pinhole model (solid lines are fits).

of the Co buffer layer is subtracted from these curves. For $N=10$, the maximum MR ratio (26%) is smaller than for $N=20$ (38%). For both values of N, the GMR ratios peak near 10 Å. Table I shows J_0 and the pinhole density x_h obtained from our calculation for $N=10$ and $N=20$. J_0 is the AF interlayer exchange for t_S in the absence of pinholes. Its value for $t_S=10$ Å is very close to those reported in Refs. 14 and 15 and in agreement with these studies, J_0 increases with decreasing t_S and is maximum for $t_S=8.3$ Å.[14,15] However, in contrast with the NiFe-Ag system, we did not try to extract an oscillation period with the Bruno-Chappert model[27] because the samples were not highly textured and the oscillatory interlayer coupling is known to be strongly dependent on the crystallographic orientation of the layers. We used the same value of the pinhole reducing coefficient α for all samples. The best fits were obtained for $\alpha=0.225$. For $N=10$, as expected, x_h increases monotonically as the spacer thickness is reduced. For $N=20$ the variation with t_S is not as clear; our calculation is probably less reliable for predicting x_h for large N because of a more complex evolution of the pinhole propagation and of the structural disorder through the multilayer.

The pinhole model can explain the shape of the magnetic hysteresis (MH) curves of Co/Cu multilayers, including the remanence observed. The density of pinholes rises rapidly below $t_S=10$ Å. A density of pinholes of a few percent leads to significant changes in the hysteresis curves. The pinhole model explains naturally a variety of hysteresis loop shapes

TABLE I. Antiferromagnetic interlayer exchange J_0, pinhole area density, and GMR ratio as a function of Cu thickness for the Cu-Co multilayers.

	$N=10$ bilayers			$N=20$ bilayers		
t_s (Å)	$-J_0$ (erg/cm^2)	x_h (%)	GMR (%)	$-J_0$ (erg/cm^2)	x_h (%)	GMR (%)
8.3	0.83	13.8	12.8	a		
8.9	0.80	13.0	17.0			
9.4				0.72	11.5	12.9
9.6	0.52	7.3	24.7			
10.0	0.44	6.6	19.8	0.42	5.1	38.7
10.5	0.24	3.8	21.8	0.34	5.1	31.5
11.1	0.16	2.4	25.9	0.25	5.2	3.1

[a]Sample not available.

without invoking biquadratic exchange. The value of J_0, the interlayer AF exchange, is still increasing for the thinnest spacer layers, 8.3 Å, even though the maximum GMR ratios occur near $t_S=10$ Å. This shows that pinholes affect the GMR curves, that the maximum in the GMR ratios does not coincide with a maximum in the interlayer AF exchange, and that the true dependence of the interlayer exchange is masked by the pinhole effects. Changes in the character of GMR curves for thin spacers, from rounded at $t_S>10$ Å to cusped at smaller spacer thickness, support this picture.

B. NiFe/Ag

Permalloy/silver multilayers were grown by triode sputtering on glass substrates cooled at 100 K with an amorphous SiO_2 buffer layer. The Ar pressure was ≈0.5 mTorr and the deposition rates were ≈1 Å/s, which led to (111)-oriented multilayers. A series of samples with $N=18$ bilayers, constant NiFe thickness ($t_M=27$ Å), and several Ag thickness around the first AF oscillation (t_S from 7.5 to 12.7 Å) were prepared. Room-temperature magnetoresistance measurements showed a maximum GMR ratio of ≈12.2% for $t_S=9.1$ Å. For $t_S>9.1$ Å, MH curves have a low remanence and a nearly linear shape characteristic of bilinear coupling. But for $t_S=7.5$, 8.3, and 9.1 Å, as shown in Fig. 10, there is a significant remanence followed by a low susceptibility magnetization curve at higher field up to the saturation field. This behavior is very similar to the one of the Cu-Co multilayers. We have fitted the magnetization curves to the pinhole model for all Ag spacer layer thickness. The results gave an increase of the AF interlayer coupling $|J|$ up to 0.09 erg/cm^2 for $t_S=7.5$ Å, but with an increasing pinhole density from $x_h=0.25\%$ for $t_S=9.1$ Å to $x_h=1.25\%$ for $t_S=7.5$ Å, while the pinhole size was kept close to 8 Å (therefore close to the Ag layer thickness). The coefficient α was found to give the best fits for a value close to 0.5. These conclusions were recently corroborated by Bouat and Rodmacq[28] with samples of better structural quality which exhibited large saturation fields for $t_S\approx 7.5$ Å.

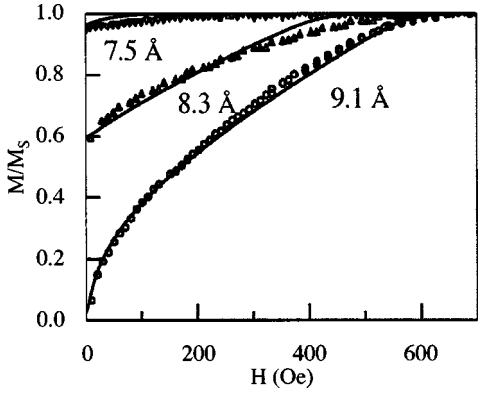

FIG. 10. Magnetization curves for NiFe-Ag multilayers around the first AF peak fitted to the pinhole model.

We were unable to observe the second AF coupling oscillation for $t_S\approx 20$ Å, and so we analyzed the oscillation based on the shape of the first AF peak, fitting the dependence of J vs t_S to the predicted oscillatory expression for a fcc Ag(111) spacer layer by Bruno and Chappert:[27]

$$J(t_S)=-\left(3I_0\frac{m^*}{m_e}\right)\left(\frac{d^2}{t_s^2}\right)\sin\left[2\pi\left(\frac{t_S}{\Lambda}\right)+\varphi\right]\exp\left(-\frac{t_S}{t_c}\right), \quad (14)$$

where I_0 (≈ -13 erg/cm^2 according to Bruno and Chappert) is the theoretical interlayer coupling prefactor, $d\approx 2.35$ Å in the lattice spacing for Ag(111), $m^*/m_0\approx 0.17$ is the reduced effective mass for Ag[111], Λ is the period of the interlayer coupling oscillations φ is the phase shift of the interlayer coupling oscillations with respect to the Rudenman-Kittel-Kasuya-Yosida (RKKY) oscillations obtained from a spherical Fermi surface, and the last exponential factor is a damping factor related to structural imperfections or roughness. t_c is a damping length characteristic of the system above which the interlayer coupling vanishes. The results of our fits to the Bruno-Chappert model are presented in Fig. 11 and summarized in Table II. We fitted the J values obtained from the pinhole model either with I_0 held constant and equal to -13 erg/cm^2 or with I_0 free. In both cases, the agreement of the pinhole model data with the theoretical predictions from the Bruno-Chappert model is better than the simple saturation-field-based determination. The lower value of t_c found for all fits and the different phase shifts φ are not major parameters according to Ref. 27. Since it was impossible to measure any significant MR at the expected position of the second AF coupling oscillation ($t_S\approx 20$–30 Å), we had to extract the periodicity of the interlayer coupling from a fitting to Eq. (14) of a smooth portion of curve with four parameters, but

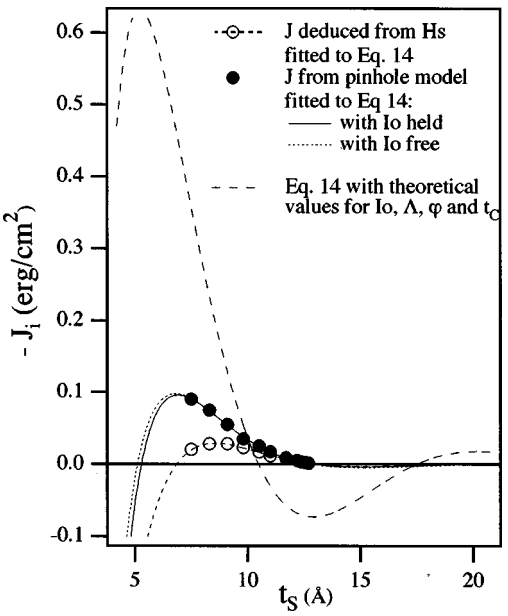

FIG. 11. Interlayer coupling strength J vs the silver thickness for NiFe-Ag multilayers fitted to the Bruno-Chappert model (solid line, Bruno-Chappert theory; open circles, data obtained from the saturation field measurement; solid circles, data obtained from the pinhole model).

the deduced value of the oscillation period is in good agreement with Ref. 27, supporting the validity of the pinhole model to extract accurate values of interlayer coupling parameters.

VII. MAGNETIC PHASE DIAGRAM FOR THE PINHOLE MODEL

A systematic computation of the magnetization curves and the spin configurations versus the ratios $\delta = d/l_i$ and $\rho = r/l_h$ was done and each magnetization curve was analyzed to extract the saturation field, remnant magnetization, and equivalent biquadratic and bilinear couplings. The parameters we chose for the identification of the various domains of the phase diagram were either h_S and m_R, which are the measured saturation field and remnant magnetization, or J_{eff} and B_{eff}, which are the apparent bilinear and biquadratic coupling factors. So we could plot these macroscopic values versus the phase space parameters δ and ρ. The agreement of the pinhole model to the biquadratic fits was also estimated as a standard deviation χ^2, each computed $m(h)$ curve being fitted to Eq. (15) [this equation relates h to m and is obtained from the minimization of Eq. (5) with respect to θ]:

$$h = \left(\frac{J_{\text{eff}}}{J}\right)\left[\left(1 - \frac{2B_{\text{eff}}}{J_{\text{eff}}}\right)m + \frac{4B_{\text{eff}}}{J_{\text{eff}}}m^3\right]. \tag{15}$$

TABLE II. Intensity of the interlayer AF coupling, oscillation period, phase shift, and damping factor for NiFe-Ag multilayers obtained from the Bruno-Chappert theory (Ref. 27), experimentally obtained from the saturation field determination and from the pinhole model (see text).

	$-I_0$ (erg/cm^2)	Λ (Å)	φ (deg)	t_C (Å)
Theory[a]	13.00	13.96	90	13.02
Deduced from H_{sat}	5.66	12.62	−14.9	4.94
Pinhole model (I_0 held)	13.00	15.29	55.5	4.32
Pinhole model (I_0 free)	10.30	15.58	62.2	4.86

[a]Reference 27.

The prefactor (J_{eff}/J) of the expression of h vs m takes into account the possibility to have a magnetization curve with a lower apparent AF coupling. The example set of calculated magnetization curves, zero-field spin configurations, and phase diagrams presented here was obtained using a ratio $l_i/a = 5$. The distance between pinholes, d_h, was changed by increasing the dimension of the mesh (total number of cells in the mesh), but not changing the number of pinholes or the cell size. By this technique, δ was varied from 0.2 (all cells have pinholes) to 2.0. The pinhole size was kept constant at $r = a$, but the effective strength of the pinhole coupling was varied by changing l_h so that ρ varied from 0.04 to 2. The remanence m_R and the saturation field h_S were calculated over this range of ρ and δ and are plotted in gray levels in Fig. 12 with ρ and δ as the coordinates defining the phase space. In Fig. 12 it is useful to divide the phase space into four different domains F, AF, AF+F, and AF*. The domain referred to as F corresponds to strong ferromagnetic coupling by the pinholes and has $m_R \approx m_S = 1$ [Fig. 13(a)]. The AF domain, by contrast, corresponds to the situation for which the pinhole coupling is weak, the spin configuration is basically antiferromagnetic, $m_R \approx 0$, and m is linear in h [Fig. 13(b)]. The AF+F domain is intermediate between F and AF. Significant regions of the film are basically AF, but there are small ferromagnetic regions near each pinhole. The spin configuration shown in Fig. 14 for $\rho = \delta = 2$ is in the AF+F area. It clearly shows the in-plane local magnetization aligned along the field axis at the pinhole surrounded by a

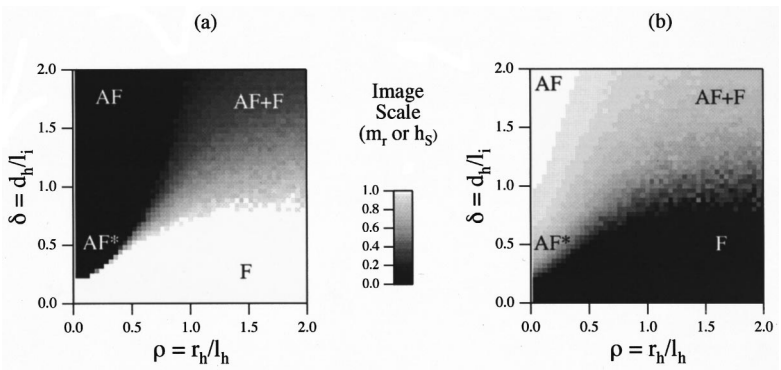

FIG. 12. Phase diagram of the pinhole model: remnant magnetization (a) and saturation field (b) of calculated magnetization curves with varying reduced pinholes sizes (ρ) and distance between pinholes (δ).

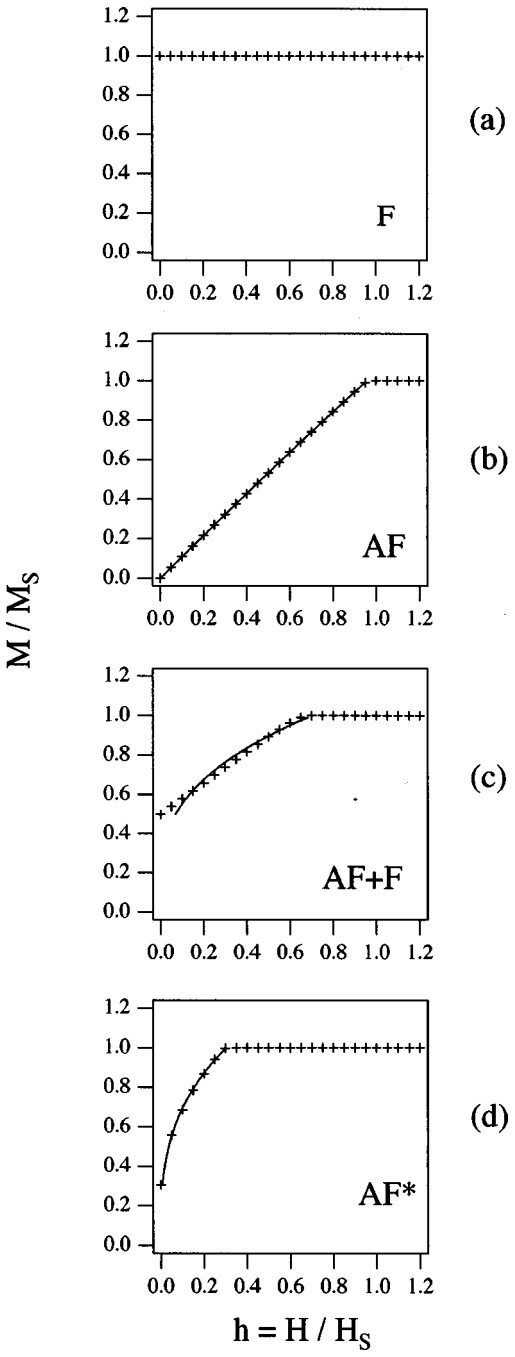

FIG. 13. Calculated magnetization curves with the pinhole model corresponding to the various situations of the phase diagram. The dashed lines are obtained with the pinhole model, while the solid lines are their best fits to the bilinear-biquadratic model (these fits are worse in the AF+F domain).

pseudowall of width ≈ 5 cells, in agreement with the ratio $l_i/a=5$. The magnetization curve in this domain shows a finite remanence followed by a magnetization linear in h [Fig. 13(c)]. We refer to this domain as an inhomogeneous domain because, within it, identifiable separate ferromagnetic and antiferromagnetic domains coexist and the magnetization curves have two distinct parts too. The boundary of the AF+F and F domains is rather sharp. Intuitively, one would expect it to correspond to the percolation limit of the pinholes which is obtained for $r=d=a$ or $\delta=l_h/l_i$, $\rho=a/l_i$. However, since the pinholes affect the magnetization in the layers over a distance l_i, the transition AF+F→F occurs for $r_h \approx l_i$ ($\delta \approx 1$ in Fig. 12).

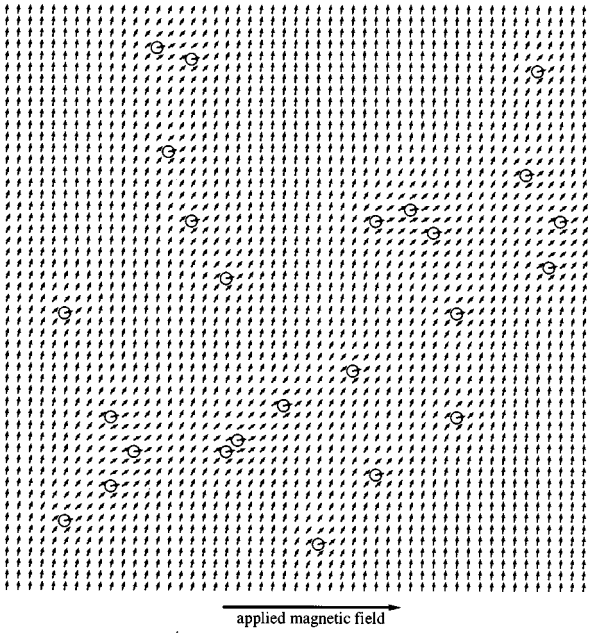

FIG. 14. Zero-field spin configuration obtained for the inhomogeneous AF+F domain of the phase diagram.

Finally, if both the AF interlayer coupling and the pinhole coupling are weak (i.e., for small values of δ and ρ), we have what we call the AF* domain. In this domain, referred to as a homogeneous domain, the pinholes are significantly coupled to one another and compete with the AF exchange for spin orientation throughout the film area. In the AF* region the remanence is small or zero and the magnetization curves are rounded with a significantly lowered saturation field. However, since this region is constrained in the lower-left corner of the phase diagram, small variations of δ or ρ induce important changes of m_R or h_S.

Note in Fig. 13 that the computed magnetization curve is best described by the biquadratic fit in the AF* domain (d) whereas the fit of the AF+F magnetization curve is bad (c). This is due to the linear slope of the inhomogeneous $m(h)$ curve which cannot be accurately simulated by the biquadratic coupling model. The image plots vs δ and ρ of B_{eff}, J_{eff}, and χ^2 are shown in Fig. 15. In Fig. 15(a), the ratio J_{eff}/J is lower than 1 for most of the calculated (ρ,δ) points, except in the AF domain. For the AF+F and AF* domains, this decrease of J_{eff} is accompanied by an increase of B_{eff} up to 30% of the initial bilinear coupling as shown in Fig. 15(b). However, the relevance of the biquadratic coupling for the pinhole model is not perfect in the AF+F domain as shown by χ^2 [Fig. 15(c)]. So the best agreement between the pinhole model and biquadratic coupling is for δ and $\rho<1$, where χ^2 is the lowest and $B_{\text{eff}}/J_{\text{eff}}$ remains non-negligible ($B_{\text{eff}}/J_{\text{eff}} \approx 0.2-0.5$). These values of δ and ρ correspond to realistic values of the dimensioned parameters for a standard multilayer (if $\delta=1$, for a pinhole size of $a \approx 10$ Å, the distance between pinholes is $d_h \approx 50$ Å and the corresponding AF interlayer coupling is $J \approx -0.4\ \text{erg/cm}^2$). This domain is

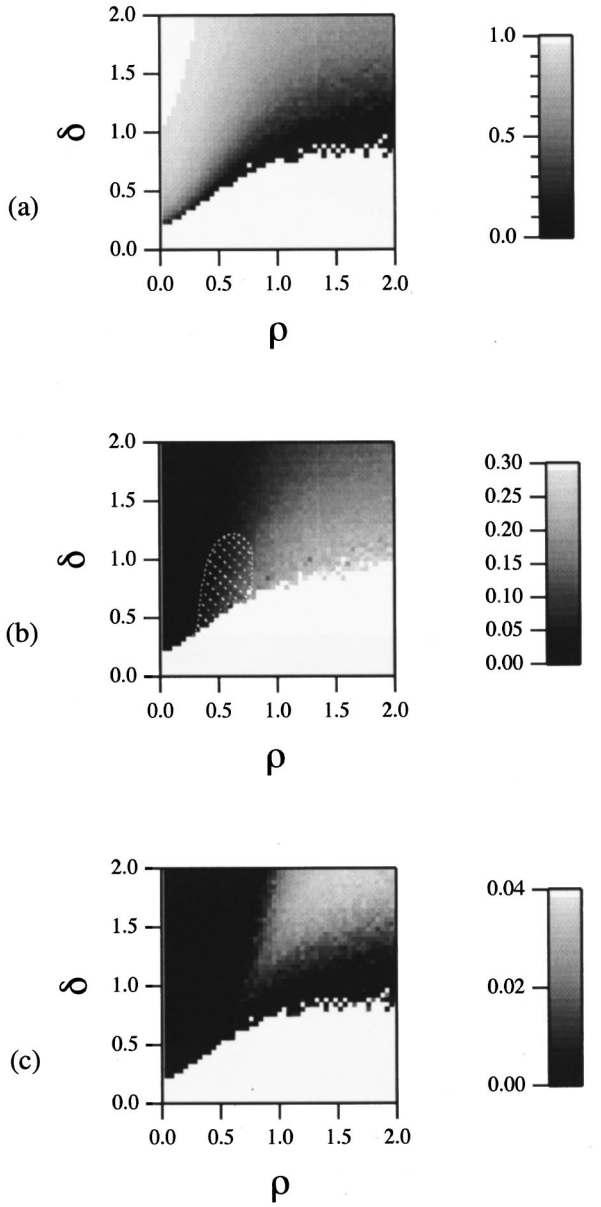

FIG. 15. Apparent bilinear coupling J_{eff} (a), biquadratic coupling B_{eff} (b), and error χ^2 between the pinhole model and the bilinear-biquadratic coupling model over the phase diagram. The dashed area in (b) corresponds to the best agreement between both models. It is located at the border between the F, AF+F, and AF* domains of the phase diagram.

close to the F domain, and small variations of the pinhole size and density via δ and ρ may strongly affect the behavior of the multilayer, causing either a dramatic reduction of the interlayer exchange coupling or even the disappearance of AF coupling in favor of a ferromagnetic apparent coupling. We think this is the reason why the GMR multilayers do not often display highly reproducible interlayer exchange coupling at low spacer layer thickness. Indeed, the defect density (pinholes, layer thickness fluctuations, etc.) is intimately related to the preparation conditions of the multilayer (high vacuum evaporation versus sputtering) and the choice of buffer layers.

VIII. DISCUSSION

Exchange-coupled multilayers with small spacer layer thickness are likely to contain pinholes, and in the previous sections, we have demonstrated that experimental magnetization curves can be simulated with our micromagnetic model based on pinhole coupling. Our model presents a limited numerical description of the influence of pinholes. For instance, we have ignored size or shape fluctuations of the pinholes, the only randomized parameter was their distance over the mesh; the effect of thermal fluctuations, studied in Ref. 20, was not treated here. Features like the domain structure of AF-coupled multilayers due to anisotropy fluctuations or magnetostatic interactions were also ignored; we assumed that the layers were infinite and the magnetization was in plane. According to Persat *et al.*,[29] during the field decrease from the saturated state of the AF-coupled bilayer, the moments of both layers may open either way (clockwise or anticlockwise) randomly over the area of the layers, generating a complex symmetry-based domain structure with the magnetization of the domain walls aligned along the applied magnetic field. These authors point out that when artificial antiferromagnetic (AAF) layers[29] are used for sensors applications, the device performance is best when the magnetization vectors in both ferromagnetic layers are perfectly antiparallel at zero field. The presence of pinholes can be a precursor for the rotational symmetry-based domain structure, generating local pinning centers for the field-aligned domain walls and leading to a decrease of the magnetic sensitivity of the devices.

Other interlayer coupling perturbations could be proposed. The first one, the so-called *orange-peel coupling*, a dipolar interaction induced by the roughness of the layers which decreases exponentially versus the spacer layer thickness was proposed by Néel in 1963.[30] However, since it is a global ferromagnetic coupling, it would just add to the antiferromagnetic bilinear coupling and reduce its strength without leading to biquadratic coupling. Furthermore, if we try to estimate the intensity of the orange-peel coupling with ferromagnetic layers having roughnesses and thicknesses similar to the ones shown in Figs. 5 and 6, we will end up with a coupling of ≈ 0.01–0.1 erg/cm^2, which is too low to actually compete with the observed AF coupling. Therefore, for small spacer thickness, orange-peel coupling is assumed to play a minor role in the modifications of interlayer exchange. The same kind of argument (too low biquadratic contribution) can be opposed to the more recent model developed by Demokritov *et al.*[31] Other features like thickness fluctuations or loose spins at the interfaces may affect the interlayer coupling (since the intensity of exchange coupling directly depends on the spacer thickness). But these are only variations of an indirect coupling and they cannot become as strong as those caused by pinholes.

IX. CONCLUSION

Our model reveals that a low pinhole area density may lead to non-negligible remanence or even to ferromagnetic apparent coupling. The pinhole model explains the shape of most of the MH curves at low spacer thickness, without introducing a biquadratic exchange term, and yields a higher

apparent value of the intrinsic bilinear interlayer coupling than the one deduced from the saturation field. This may reconcile the discrepancy between theoretical models and experimental data. As shown in the case of NiFe-Ag multilayers, the oscillation periodicity of the interlayer coupling deduced from the pinhole model also leads to values in better agreement with theoretical models. Finally, we have shown in this paper that a distribution of ferromagnetic point defects—the pinholes—is a good approach to describe the behavior of real multilayers and it is likely to appear when the spacing layers are of a few atomic planes.

ACKNOWLEDGMENTS

The authors acknowledge Dr. B. Rodmacq and Dr. J. Pierre for technical support and fruitful discussions. Support for this work from CNRS and NATO under Grant No. CRG 971645 is also acknowledged.

[1] S. S. P. Parkin, Phys. Rev. Lett. **67**, 3598 (1991).
[2] M. N. Baibich, J. M. Broto, A. Fert, F. Nguyen van Dau, F. Petroff, P. Etienne, G. Creuzet, A. Friederich, and J. Chazelas, Phys. Rev. Lett. **61**, 2472 (1988).
[3] S. S. P. Parkin, N. More, and K. Roche, Phys. Rev. Lett. **64**, 2304 (1990).
[4] R. E. Camley and J. Barnas, Phys. Rev. Lett. **63**, 664 (1989).
[5] B. Dieny, V. S. Speriosu, S. S. P. Parkin, B. A. Gurney, D. R. Wilhoit, and D. Mauri, Phys. Rev. B **43**, 1297 (1991).
[6] M. Rührig, R. Schäfer, A. Hubert, R. Mosler, J. A. Wolf, S. Demokritov, and P. Grünberg, Phys. Status Solidi A **125**, 635 (1991).
[7] B. Rodmacq, K. Dumesnil, Ph. Mangin, and M. Hennion, Phys. Rev. B **48**, 3556 (1993).
[8] P. Bruno, J. Magn. Magn. Mater. **121**, 248 (1993).
[9] J. C. Slonczewski, Phys. Rev. Lett. **67**, 3172 (1991).
[10] H. Fujiwara and M. R. Parker, J. Magn. Magn. Mater. **135**, L23 (1994); H. Fujiwara, W. D. Doyle, A. Matsuzono, and M. R. Parker, *ibid.* **140-144**, 519 (1995).
[11] J. J. Krebs, G. A. Prinz, M. E. Filipkowski, and C. J. Gutierrez, J. Appl. Phys. **79**, 4525 (1996).
[12] U. Gradmann and H. J. Elmers, J. Magn. Magn. Mater. **137**, 44 (1994).
[13] O. Massenet, F. Biragnet, H. Juretschke, R. Montmory, and A. Yelon, IEEE Trans. Magn. **MAG-2**, 533 (1966).
[14] J. F. Bobo, L. Hennet, M. Piecuch, and J. Hubsch, J. Phys.: Condens. Matter **6**, 2689 (1994).
[15] B. Heinrich and J. F. Cochran, Adv. Phys. **42**, 523 (1993) and references therein.
[16] This assumption is based on the fact that for very thin films, the aspect ratio of the pinhole is not too unfavorable (limited gain in demagnetizing energy if the magnetic moments are perpendicular to the films in the pinhole), but the loss in exchange energy at the two interfaces with the magnetic layers is very large. If one assumes a total loss of the demagnetizing energy (the volume of the pinhole multiplied by the square of the saturated magnetization), this energy will only compensate the energy needed to restore the in plane magnetic moment in magnetic film for a thickness of the order of 10 nm for the individual films.
[17] W. F. Brown, *Magnetostatic Principle in Ferromagnetism* (North-Holland, Amsterdam, 1962).
[18] A. S. Arrott and B. Heinrich, J. Magn. Magn. Mater. **93**, 571 (1991).
[19] J. Kohlhepp, M. Valkier, A. van der Graaf, and F. J. A. den Broeder, Phys. Rev. B **55**, R696 (1997).
[20] D. B. Fulghum and R. E. Camley, Phys. Rev. B **52**, 13 436 (1995).
[21] J. F. Bobo, H. Fischer, and M. Piecuch, in *Magnetic Ultrathin Films: Multilayers and Surfaces Interfaces and Characterization*, edited by B. T. Jonker, S. A. Chambers, R. F. C. Farrow, C. Chappert, R. Clarke, W. J. M. de Jonge, T. Egami, P. Grünberg, K. M. Krishnan, E. E. Marinero, C. Kau, and S. Tsunashima, MRS Symposia Proceedings No. 313 (Materials Research Society, Pittsburgh, 1993), p. 467.
[22] The source code and compiled application for workstation or Macintosh is available on request from the authors.
[23] J. F. Bobo, M. Piecuch, and E. Snoeck, J. Magn. Magn. Mater. **126**, 440 (1993); J. F. Bobo, E. Snoeck, M. Piecuch, and M-J. Casanove, in *Polycrystalline Thin Films: Structure, Texture, Properties and Applications*, edited by K. Barmak, M. A. Parker, J. A. Floro, R. Sinclair, and D. A. Smith, MRS Symposia Proceedings No. 343 (Materials Research Society, Pittsburgh, 1994), p. 423.
[24] J. F. Bobo, B. Baylac, L. Hennet, O. Lenoble, M. Piecuch, B. Raquet, and J-C. Ousset, J. Magn. Magn. Mater. **121**, 291 (1993).
[25] John C. Spence, *Experimental High Resolution Electron Microscopy* (Clarendon, Oxford, 1981).
[26] H. Kikuchi, J. F. Bobo, and R. L. White, IEEE Trans. Magn. **MAG-33**, 3583 (1997).
[27] P. Bruno and C. Chappert, Phys. Rev. Lett. **67**, 1602 (1991); **67**, 2592(E) (1991); Phys. Rev. B **46**, 261 (1992).
[28] S. Bouat and B. Rodmacq (private communication).
[29] N. Persat, H. A. M. van den Berg, K. Cherifi-Kodjaoui, and A. Dinia, J. Appl. Phys. **81**, 4748 (1997).
[30] L. Néel, C. R. Hebd. Seances Acad. Sci. **255**, 1676 (1962).
[31] S. Demokritov, E. Tsympbal P. Grünberg W. Zinn, and Y. K. Schuller, Phys. Rev. B **49**, 720 (1993).